The behaviour of charged particles (ions) during new particle formation events in urban Leipzig (Germany)

Alex Rowell[1], James Brean[1], David C.S. Beddows[1], Zongbo Shi[1], Avinash Kumar[2], Matti Rissanen[2,3], Miikka Dal Maso[4], Peter Mettke[5], Kay Weinhold[5], Maik Merkel[5], Roy M. Harrison[1,6]

[1]School of Geography, Earth & Environmental Sciences, University of Birmingham, Birmingham B15 2TT, United Kingdom
[2]Aerosol Physics Laboratory, Physics Unit, Tampere University, 33720 Tampere, Finland
[3]Department of Chemistry, University of Helsinki, P. O. Box 55, Helsinki, Finland
[4]Department of Physics, Tampere University of Technology, P.O. Box 692, 33100 Tampere, Finland
[5]Leibniz Institute for Tropospheric Research (TROPOS), Atmospheric Chemistry Department (ACD), Permoserstr. 15, 04318 Leipzig, Germany
[6]Department of Environmental Sciences, Faculty of Meteorology, Environment and Arid Land Agriculture, King Abdulaziz University, Jeddah 21589, Saudi Arabia

Correspondence to: Roy M. Harrison (r.m.harrison@bham.ac.uk)

ABSTRACT

Air ions are electrically charged particles in air. They are ubiquitous in the natural environment and affect the earths radiation budget by accelerating the formation and growth of new aerosol particles. Despite this, few datasets exist exploring these effects in the urban environment. A Neutral cluster and Air Ion Spectrometer was deployed in Leipzig, Germany, to measure the number size distribution of charged particles from 0.8 to 42 nm, between July 27th and August 25th 2022. Following previous analyses, charged particles were classified into small (0.8–1.6 nm), intermediate (1.6–7.5 nm), and large (7.5–22 nm) fractions by mass diameter and their mean concentrations (sum of positive and negative polarities) during the campaign were 405, 71.6, and 415 cm^{-3}, respectively. The largest peaks in intermediate and large ions were explained by New Particle Formation (NPF), with intermediate ions correlating well with sulphuric acid dimer. Smaller morning and evening peaks were coincident with black carbon concentrations, and attributed to primary emissions. NPF events, observed on 30% of days, coincided with intense solar radiation and elevated sulphuric acid dimer. Small charged particles were primarily associated with radioactive decay and highest during the early hours, and are unrelated to primary emissions or NPF. The apparent contributions of charged particles to 3

and 7.5 nm particle formation rates were 5.7 and 12.7%, respectively, respectively, with mean growth rates of 4.0 nm h^{-1} between 3-7.5 nm and 5.2 nm h^{-1} between 7.5-22 nm. The ratio of charged to total particle formation rates at 3 nm suggests a minor role for charged particles in NPF. We conclude that NPF is a primary source of >3 nm ions in our data, with primary emissions being the major source in the absence of NPF.

1. INTRODUCTION

Atmospheric aerosol particles influence the Earth's energy budget (Carslaw et al., 2013; Quaas et al., 2009), impair visibility (e.g. haze events, aerosol–fog interactions, and cloud formation) (Boutle et al., 2018; Tian et al., 2016), and adversely impact human health through the degradation of air quality (Kelly and Fussell, 2015). The environmental impacts and health effects of aerosol particles are dependent on their number concentration, size, structure, chemical composition, and charge state. These properties, however, vary spatially and temporally (Seinfeld and Pandis, 2016).

New particle formation (NPF) accounts for a large fraction of global aerosol production (Gordon et al., 2017; Spracklen et al., 2010). NPF is a phenomenon observed in many different environments around the world, from pristine remote locations to polluted urban atmospheres (Brean et al., 2021, 2023; Uusitalo et al., 2021; Yao et al., 2018). It is an important atmospheric process wherein gas-phase molecules cluster together and grow to form new aerosol particles. Charged particles can play an important role in the enhancement of these formation and growth processes (Kirkby et al., 2023).

Charged particles, also referred to as air ions, are electrically charged atoms, molecules, clusters of molecules, or aerosols in the atmosphere, which can influence NPF processes. These charged particles can be positively or negatively charged, depending on whether a particle has gained or lost an electron. They can promote the formation of small molecular clusters, enhance their stability, and decrease their evaporation rate (He et al., 2021; Kirkby et al., 2011). Following nucleation and the formation of stable new particles, ion-induced condensation can accelerate particle growth (Svensmark et al., 2017).

Various environmental factors impact the production and removal of air ions and charged particles in the atmosphere. Sources include cosmic rays (Svensmark et al., 2017), radioactive

decay (Zhang et al., 2011), traffic (Jayaratne et al., 2014), transmissions lines (Jayaratne et al., 2011), volcanic eruptions (Rose et al., 2019), thunderstorms and lightning (J-P Borra et al., 1997), solar radiation (Vana et al., 2008; Wang et al., 2005), vegetation (Wang and Li, 2009), and splashing water (Tammet et al., 2009). Sinks involve redistribution via coagulation with

70   pre–existing aerosol (Mahfouz and Donahue, 2021), losses via ion–ion recombination (Zauner-Wieczorek et al., 2022) and dry deposition (Tammet et al., 2006).

Several studies have investigated the role of ions in the nucleation process, yielding varied results. Manninen et al. (2010) found that contributions of ion–induced nucleation to total par-

75   ticle formation at 2 nm were typically in the range of 1–30% between 12 field sites across Europe. In remote locations, Kulmala et al. (2010) found that contributions were typically significantly less than 10% in Hyytiälä (Finland), Hohenpeissenberg (Germany), and Melpitz (Germany). In urban locations, contributions were observed at approximately 1.3% at 1.5/2 nm in Helsinki, Finland (Gagné et al., 2012) and 10% at 3 nm in Brisbane, Australia (Pushpawela

80   et al., 2018). However, few comprehensive analyses of the temporal variation of charged particles, together with their contribution to particle formation and growth in the urban environment, have been published to date.

Here, the daily cycles, sources, and sinks of charged particles, as well as their contributions to

85   new particle formation and growth rates were investigated in a summertime urban environment. A Neutral cluster and Air Ion Spectrometer was deployed at an urban background site in Leipzig, Germany, to measure the mobility distribution of neutral and charged particles, between 27th July and 25th August 2022. The urban background site is located in the Leibniz Institute for Tropospheric Research, a renowned centre specialising in both in–situ and remote observa-

90   tions of aerosols and clouds. The air ion/charged particle population was classified into small (0.8–1.6 nm mass diameter, 1.1—1.9 nm electrical mobility diameter), intermediate (1.6–7.5 nm mass diameter, 1.9—7.8 nm electrical mobility diameter), and large particles (7.5–22 nm mass diameter, 7.8 – 22.3 nm electrical mobility diameter) for analysis, following the classification system outlined by Tammet (2006).

2. MATERIALS AND METHODS

2.1. Site description

Leipzig is located in the German State of Saxony in east Germany. Leipzig is the 8th most populated city in Germany, with 0.6 million inhabitants. The measurements were located at the Leibniz Institute for Tropospheric Research (denoted as Leipzig–TROPOS) (N51°21'09", E12°26'04", 127 m above mean sea level) within the Leipzig Science Park (**Figure 1**), from 27th July to 25th August 2022. The charged and neutral particle measurements were taken from a laboratory on the fourth floor of an institute building positioned centrally within the Science Park, approximately 10 meters from ground level. Leipzig–TROPOS is located approximately 100 m from a number of highly–trafficked roads and is classified as an urban background site. The Science Park contains other research institutes and related companies, allotted parking bays, including a multi–storey carpark, and greenspace. The park perimeter includes transport infrastructure (including road, rail, and tramways), commercial property (e.g. restaurants, hotels, a petrol station etc.), residential property, on–street parking, and additional greenspace. The solar maximum was at 13:00 local time. Local time was UTC+2, and all times reported here onwards are in local time.
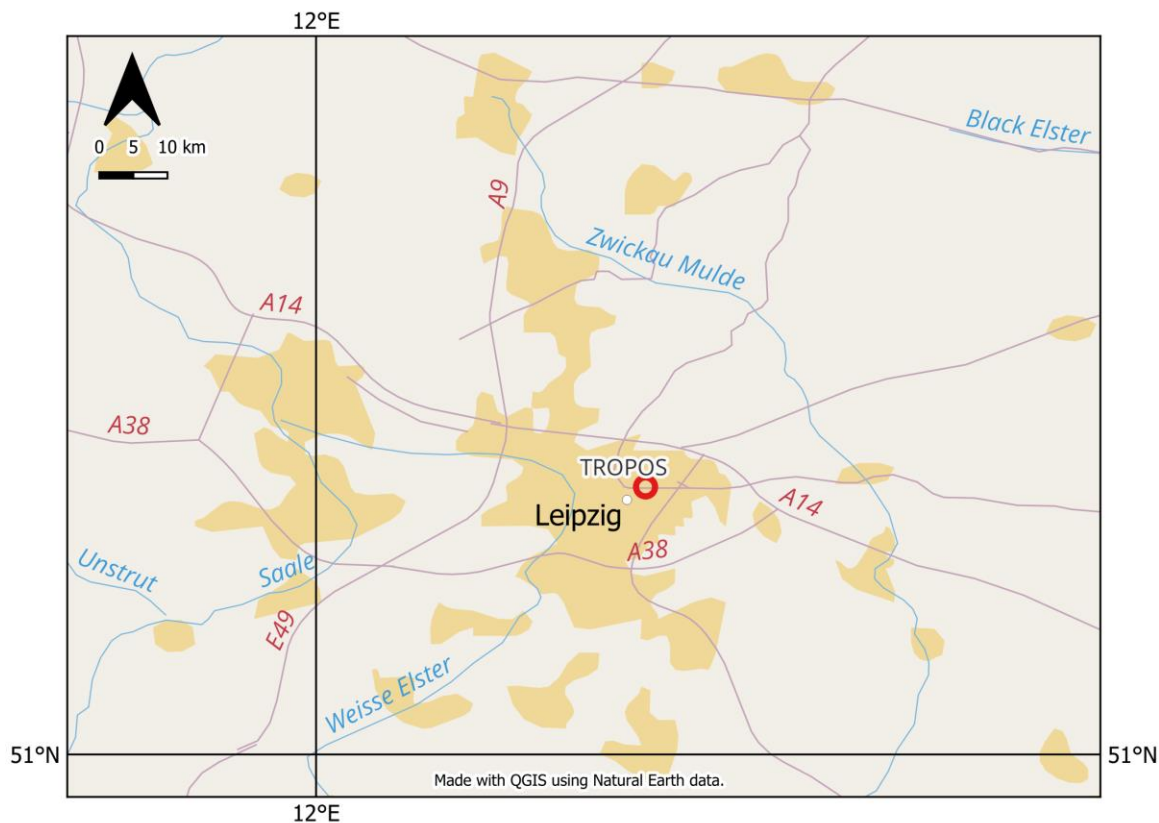
Figure 1: Location of the TROPOS site (red marker), approximately 4 km northeast of Leipzig city centre.

2.2. Meteorological conditions

Leipzig has a temperate continental climate. The weather of the city can be highly variable as it is exposed to both cold and warm air masses and thunderstorms are not uncommon during the warm season (May through August). Weather–related measurements were taken from a meteorological station on the roof of the same institute building accommodating the air quality–related instruments at Leipzig–TROPOS. From June to August 2022, persistent heatwaves affected many parts of Europe, including Germany. The mean hourly air temperature during the campaign was 22.4 °C and the highest hourly air temperature was 37.1 °C recorded on the 4th August 2022.

2.3. Description of the instruments

2.3.1. Neutral cluster and Air Ion Spectrometer

The principle of the Neutral cluster and Air Ion Spectrometer (NAIS, Ariel Ltd., Estonia) is described in detail by Mirme and Mirme (2013). A NAIS was used to measure the particle number size distribution (PNSD) of naturally charged, and also the sum of naturally charged

and neutral particles from 0.8–42 nm (3.2 to 0.0013 cm^2 V^{-1} s^{-1}) by their mobilities. From here onwards we refer to all diameters as mass diameters for consistency with the literature (e.g. Tammet et al., 2006; Ku & Fernandez de la Mora, 2009). In the case of the charged and neutral particles, the data from 3-42 nm is used, as the charging mechanism for neutral particles causes interference <3 nm. Neutral and charged measurements will hereon be referred to as simply "total", and the total measurements were taken from the negative column. The instrument was comprised of two multichannel differential mobility analyser (DMA) columns, one for each polarity. Both columns had a software–controlled sample preconditioning unit which allowed the instrument to switch between detecting naturally charged particles or total particles. The sheath air flow rate was approximately 60 L min^{-1} and the total sample flow rate was 54 L min^{-1} (divided equally between both DMAs). The time resolution per complete distribution was five–minutes. Here, we refer to all charged particles measured by the NAIS as "charged particles", which includes charged aerosols, as well as charged molecules and charged clusters of molecules.

2.3.2. Custom–built mobility particle size spectrometer

The principle of the mobility particle size spectrometer (MPSS) is described in detail by Wiedensohler et al. (2012). A custom–built MPSS was used to measure the PNSD (from 5 to 800 nm) for the duration of the measurement campaign. The instrument was comprised of a bipolar diffusion charger (^{85}Kr neutraliser), a Vienna–type DMA (electrode length 280 mm), and a condensation particle counter (CPC model 3772, TSI Inc., USA). The sheath air flow rate (5 L min^{-1}) to sample air flow rate (1 L min^{-1}) was operated at a ratio of 5:1. Both the aerosol sample flow and sheath air flow were actively dried. Particle losses were quantified and accounted for in the final size distribution. The time resolution for one combined upscan and downscan was ten–minutes, and the instrument alternated between measuring the total PNSD and the non-volatile PNSD, giving a measurement of the total PNSD every twenty minutes.

2.3.3. Other instrumentation

The Tampere University nitrate Chemical Ionisation–Atmospheric Pressure interface–Time of Flight mass spectrometer (nitrate CI–APi–ToF) was used to measure neutral H_2SO_4 and (H_2SO_4) $_nHSO_4^-$ clusters for the duration of the measurement campaign. The instrument is highly sensitive to strongly acidic compounds, as well as compounds with two hydrogen bond donor groups in the gas phase (Hyttinen et al., 2015). The front end consists of a chemical

160   ionisation system where a ca. ~8 L min^{-1} sample flow is drawn in through a 1 m length ¾" OD

stainless steel tube, where it enters an ionising chamber. Inside the chamber, a secondary flow

is run parallel and concentric to the sample flow, rendering the reaction chamber effectively

wall–less. A 10 cm^3 min^{-1} flow of a carrier gas (in this case, N_2) is passed over a reservoir of

liquid HNO_3, entraining vapour which is subsequently ionised to NO_3^- via an X–ray source.

165   The nitrate ions are then guided into the sample flow by an electric field where they charge

molecules by clustering or proton transfer. The sample enters the critical orifice at the front

end of the instrument at 0.8 L min^{-1} and are guided through a series of differentially pumped

chambers before they reach the ToF analyser. Data analysis was carried out in the Igor Pro 9.

Dried and filtered compressed air was used for the sheath flows.

170

The instrument was calibrated with respect to sulphuric acid (Kürten et al., 2012). The quanti-

fication of sulphuric acid in the nitrate CI–APi–ToF is as follows:

$$[H_2SO_4] = C \times \ln\left(1 + \left(\frac{H_2SO_4NO_3^- + HSO_4^-}{\sum_{n=0-2}(HNO_3)_n NO_3^-}\right)\right) \tag{1}$$

where C is a calibration constant, here $1.07 \cdot 10^9$ cm^{-3} for the instrument. Presuming that all

175   collisions between analyte *A* and the reagent ion result in charging via clustering or deprotona-

tion, the production of charged analytes will continue at the kinetic limit for H_2SO_4. Blanks

were performed mid-campaign. Blank signals were negligible for all compounds of interest.

Black Carbon (BC) was measured through the attenuation of 880 nm light with an Aethalom-

eter (AE33, Magee Scientific, USA) using the default mass absorption coefficient.

180   **2.4. Condensation sink, formation and growth rates**

NPF events were identified visually based on the time evolution of the PNSD plotted as contour

plots using the criteria of Dal Maso et al. (2005). Measurement days were classified into three

categories: NPF event, undefined, and non–NPF event according to methods described by Dal

Maso et al. (2005). NPF event days were classified as such when days showed both particle

185   formation and growth. Equally, undefined days were assigned when days satisfied some but

not all of the aforementioned criteria (i.e. a new but non–persistent mode or no clear signs of

growth). Lastly, non–NPF event days were grouped as such when the total PNSD data showed

no clear indication of new particle formation.

Each plot contained data spanning 24 hours and ranging from 0.8–42 nm (charged PNSD from

190   the NAIS) and 3–800 nm (neutral and charged PNSD from the NAIS and custom–built MPSS,

utilising the NAIS <20 nm and the MPSS >20 nm). Example plot in **Figure S1**. All NPF

signatures were seen simultaneously in the PNSD and charged PNSD simultaneously. Each day was plotted using a perceptually uniform, high contrast colour palette (Mikhailov, 2019).

The condensation sink (CS) represents the rate at which a vapour phase molecule will collide with pre–existing particle surface, and was calculated from the MPSS data as follows (Kulmala et al., 2012):

$$CS = 2\pi D \cdot \sum_{d_p} \beta_{m,d_p} \cdot d_p \cdot N_{d_p} \tag{2}$$

where D is the diffusion coefficient of the diffusing vapour (assumed to be sulphuric acid), β_m is a transition regime correction, $\underline{d_p}$ is particle diameter, and N_{dp} is the number of particles at diameter d_p. The formation rate of new particles at size dp (J_{dp}) is calculated as follows, presuming a homogeneous airmass:

$$J_{d_p} = \frac{dN_{d_p}}{dt} + CoagS_{d_p} \cdot N_{d_p} + \frac{GR}{\Delta d_p} . N_{d_p} \tag{3}$$

where the first term on the right–hand side represents the rate at which particles enter the size d_p, and the second term refers to losses from this size by coagulation ($CoagS_{dp}$ being the coagulation sink at size d_p, and N_{dp} being the number of particles at size d_p, calculated according to Cai and Jiang (2017)), with the third term referring to losses from this size by growth. When calculating the formation rate, instead of using a single particle size, a range is used. In this paper we use two ranges, 3–7.5 nm for 3 nm particles, and 7.5–22 nm for 7.5 nm particles. These sizes were chosen for consistency with the size–cuts used for the rest of the analyses. The formation rate of charged particles involves two additional terms, and is as follows:

$$J_{d_p}^{\mp} = \frac{dN_{d_p}^{\mp}}{dt} + CoagS_{d_p} \cdot N_{d_p}^{\mp} + \frac{GR}{\Delta d_p} \cdot N_{d_p}^{\mp} + \alpha \cdot N_{d_p}^{\mp} \cdot N_{<d_{p-upper}}^{\pm} - \beta \cdot N_{d_p} \cdot N_{<d_{p-lower}}^{\mp} \tag{4}$$

Where the fourth term accounts for the loss of charged particles due to their recombination with other charged particles of the opposite polarity below the upper bound of d_p, and the fifth term accounts for the gain of charged particles caused by the attachment of charged particles below the lower bound of d_p with neutral clusters (Yan et al., 2018). The growth rate (GR) of new particles, which is the change of dp over time of new particles here calculated by the mode–fitting method (Kulmala et al., 2012).

3. RESULTS AND DISCUSSION

3.1. Number concentrations of charged particles

Table 1 shows a statistical summary of small, intermediate, and large charged particle concentrations at Leipzig–TROPOS. Mean number concentrations of small charged particles (0.8–1.6

nm) were 305 and 100 cm^{-3} for positive and negative polarities, respectively. Observed concentrations are comparable with, albeit on the lower end of, the typical tropospheric range reported by Hirsikko et al. (2011). The comparatively low concentrations are in line with the higher coagulation sink for small particles in the urban environment, which is expected to reduce the average concentration. The positive particle concentrations are roughly a factor of 3 greater than the negative particle concentrations, and this is consistent across the 5-95% spread, so is not attributable to spikes in positive charged particles (see mean charged PNSD in **Figure 2a**). Similar disparities between small charged particles of opposing polarities have been documented in the literature. A measurement campaign in Saare County, Estonia between July and September 1984 reported mean concentrations of positively and negatively charged small particles of 261 and 173 cm^{-3}, respectively (Hõrrak, 1987). The imbalance is believed to be caused by the Earth's negatively charged surface impacting the distribution of charged particles, referred to as the electrode effect (Hoppel, 1967; Hõrrak et al., 2003). This effect is closest to the ground, and tapers off strongly at a height of meters (Hõrrak et al., 2003). This may also be due to a charged surface on the wall near the inlet, or the inlet itself.

Table 1: Statistical summary of small (0.8–1.6 nm), intermediate (1.6–7.5 nm), and large (7.5–22 nm) charged particle number concentrations per cm^{-3}. Data coverage: 27th July 2022 14:00 to 25th August 2022 08:00 (UTC) using hourly means.

	Mean	Median	5-95%
Small (+)	305	299	193 - 451
Small (-)	100	96.2	45.3 - 173
Intermediate (+)	30.7	12.4	1.36 - 132
Intermediate (-)	40.9	18.9	6.24 - 174
Large (+)	205	147	43.8 - 611
Large(-)	210	152	54.9 - 620
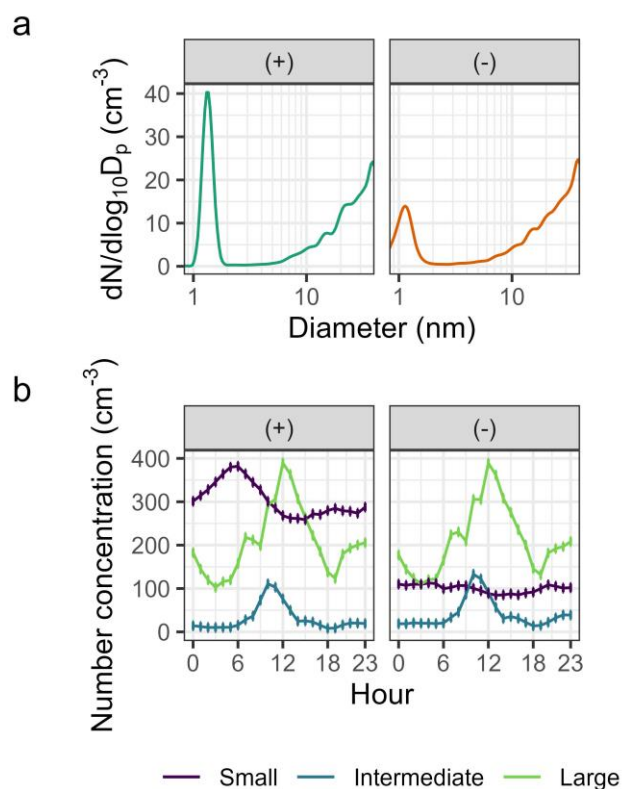
Figure 2: (a) Mean size distribution of positive and negatively charged particles between 0.8 and 22 nm. (b) Mean diurnal cycles of small (0.8–1.6 nm), intermediate (1.6–7.5 nm), and large (7.5–22 nm) charged particles. The vertical lines represent the standard error of the mean.

Mean concentrations of intermediate charged particles (1.6–7.5 nm), on the other hand, were comparatively very low. Mean number concentrations of intermediate charged particles were 30.7 and 40.9 cm^{-3} for positive and negative polarities, respectively. Negative particles show greater spread, with the lower 5% and lower mean counts possibly also attributable to the electrode effect. Observations are very similar to annual mean concentrations (35-40 cm^{-3} for each polarity) recorded between April 2010 and November 2011 in Tartu, Estonia by Tammet et al. (2014). Though, they are approximately 2 times higher (depending on polarity, with higher negative concentrations) than mean concentrations recorded between June 2009 and October 2010 in Paris, France by Dos Santos et al. (2015). The differences between these studies may be explained by proximity to and density of the surrounding transport infrastructure (see **section 3.2.**), photochemical processes (see **section 3.5.**), and length of campaign period.

Much like intermediate charged particles, there was little difference in mean concentrations between the opposing polarities of large charged particles (7.5–22 nm). However, mean concentrations of large charged particles (during the whole campaign) were considerably higher than intermediate charged particles. Mean number concentrations were 210 and 205 cm^{-3} for positive and negative polarities, respectively, and were approximately 5-6 times higher (depending on polarity, higher for positive particles) than intermediate charged particles. The spread in large ion counts is similar between positive and negative charged particles, and the relative magnitude of this spread is similar to the intermediate ions.

3.2. Diurnal cycles of charged particles

Figure 2b shows the mean diurnal cycles of small, intermediate, and large charged particles at Leipzig–TROPOS. Small charged particle concentrations peaked in the early morning (05:00–06:00), decreased into the afternoon (11:00–13:00), and increased into the night. Such observations are comparable to other studies in Pune, India (Dhanorkar and Kamra, 1994), Tumbarumba, Australia (Suni et al., 2008), and Paris, France (Dos Santos et al., 2015) and may be attributed to fluctuations in boundary layer mixing height and the accumulation of radioactive gases (e.g. radon). Concentrations of small charged particles increased prior to the below–mentioned peaks in intermediate and large charged particle concentrations and decreased thereafter. Diurnal cycles suggest that small charged particles arise primarily from natural processes and are quickly lost via recombination and attachment to larger aerosols. The main natural ion production processes are cosmic radiation and radioactive decay. Cosmic ray intensity is fairly constant throughout the lower atmosphere (Mercer and Wilson, 1965), while the variations in radon concentrations is attributable to boundary layer dynamics (Čeliković et al., 2023). The diurnal variation we observe is therefore likely to be a combination of boundary layer height changes affecting the radon concentrations, and therefore source strength, and variations in particle number surface area altering loss rates due to coagulation due to both boundary layer height changes and primary and secondary particle emissions.

Intermediate charged particle concentrations peaked several hours after the initial peak in small charged particles (10:00) and again later in the day (22:00). Similarly, large charged particle concentrations peaked at midday (12:00) and lesser peaks were observed in the morning (07:00–08:00) and in the evening/night–time (23:00). Before-midday, and midday (10:00 for intermediate, 12:00 for large) peaks in both classifications coincided with intense solar radiation (see **section 3.4.**) and occurred when NPF events were observed (see **section 3.5.**). Lesser

peaks coincided with busy road traffic periods and economic activities, known to emit high quantities of positive and negative charged particles (Jayaratne et al., 2010, 2014; Thomas et al., 2024). Pollution–related peaks appeared more pronounced in the large charged fraction. Diurnal cycles suggest photochemistry and local air pollution dominate intermediate and large charged particle production, with the latter contributing more significantly to large charged particle concentrations.

3.3. Frequency of new particle formation

A total of 9 NPF event, 6 undefined, and 15 non–NPF event days were identified across the 30–day measurement campaign at Leipzig–TROPOS. The frequency of NPF event days (30%) was comparable with frequencies from long–term analysis of summertime data at this site (Bousiotis et al., 2021).

3.4. Meteorology and charged particles

Figure 3 shows the correlation coefficients between charged particles in different diameter classifications and meteorological variables at Leipzig–TROPOS. Individual scatterplots available in **Figure S2**. Solar radiation and air temperature exhibited negative correlations with small charged particles but positive correlations with intermediate and large charged particles. Conversely, relative humidity showed positive correlations with small charged particles and negative correlations with intermediate and large charged particles. Air temperature is typically elevated when solar radiation is high, and relative humidity is typically inversely related with air temperature (Seinfeld and Pandis, 2016). Fluctuations in boundary layer mixing height, the accumulation of radioactive gases, and the CS, discussed in **section 3.2.**, are believed to have influenced the small charged fraction. Mixing layer height is influenced by air temperature, with cooler morning temperatures theoretically limiting vertical mixing (Seinfeld and Pandis, 2016) and inadvertently enhancing small charged particle concentrations.
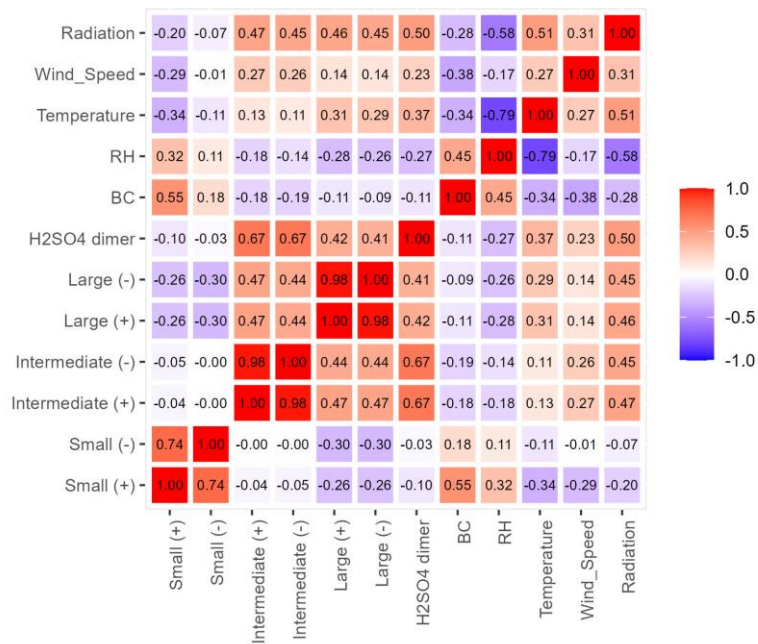
Figure 3: Pearson correlation matrix heatmap of meteorological variables (solar radiation, air temperature, relative humidity, and wind speed) and small, intermediate, large, and total charged particles (of both polarities). Also include are H₂SO₄ dimer and BC. Warm colours (red) represent positive correlations, and cold colours (blue) represent negative correlations. Correlation strength ranges from -1 to +1. The shade indicates the strength of the correlation, with darker shades indicating stronger correlations. Data coverage: 27th July 2022 14:00 to 25 August 2022 08:00 (UTC) using hourly means. Individual scatterplots available in Figure S2.

3.5. Diurnal cycles of charged particles during new particle formation

Figure 4a,c,e shows the mean diurnal cycles of small, intermediate, and large charged particles on NPF event, undefined, and non–NPF event days at Leipzig–TROPOS. On NPF event days, diurnal maxima of small charged particles were observed between 05:00 and 08:00 and minima between 14:00 and 16:00. These diurnal cycles are unrelated to NPF. Diurnal maxima of intermediate and large charged particles were observed at 10:00 and 12:00, respectively. Time–gaps between maximum concentrations of intermediate and large charged particles (approximately two hours) likely indicate growth between size classifications, a phenomenon not observed on non–NPF event days (alternative graphic presented in **Figure S4**). Comparable time–gaps have been observed in both urban (Dos Santos et al., 2015) and rural (Hõrrak et al., 2003) settings. Small charged particle concentrations were lower on NPF event days compared to non–NPF event days, consistent with findings in rural areas (Gagné et al., 2010; Hõrrak et al., 2003), possibly due to stronger vertical mixing and a deeper boundary layer. In contrast, maximum concentrations of intermediate and large charged particles were approximately 4.0–4.4 and

340   3.6–3.7 times higher (depending on polarity, higher for negative particles), respectively, on

NPF event days compared to non–NPF event days.
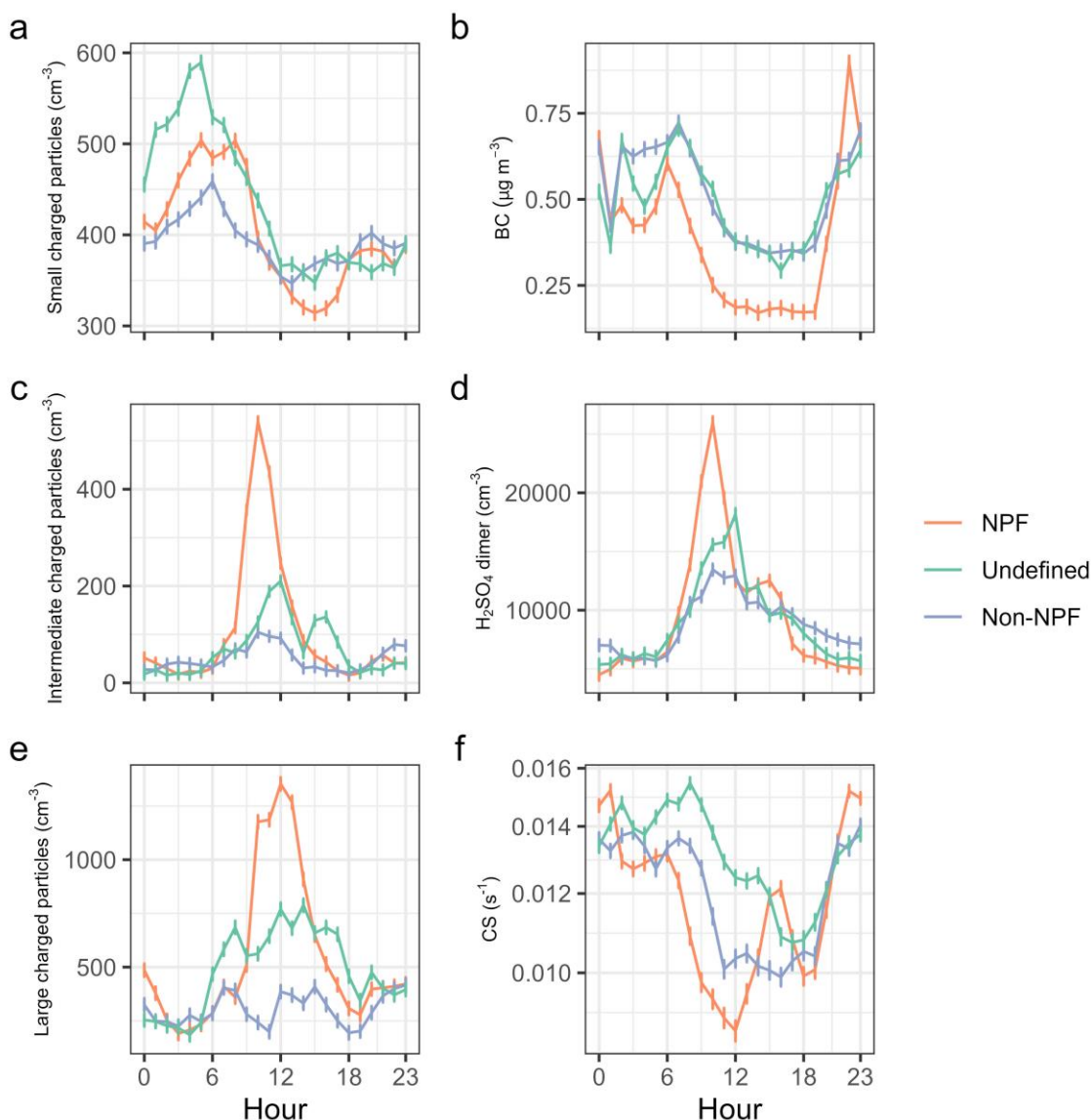
345   **Figure 4: Mean diurnal cycles of (a) small (0.8–1.6 nm), (c) intermediate (1.6–7.5 nm), and (e) large (7.5–22 nm) charged particles, as well as (b) BC, (d) H₂SO₄ dimer, and (f) CS on new particle formation (NPF) event, undefined, and non–NPF event days. The vertical lines represent the standard error of the mean.**

350   The mean diurnal cycles of black carbon, sulphuric acid (H_2SO_4) dimer, and condensation sink

(CS) concentrations on NPF event, undefined, and non–NPF event days at Leipzig–TROPOS

are shown in **Figure 4b,d,f**. BC concentrations were generally lower in the morning and into

the early evening, and noticeably higher in the late evening/night–time on NPF event days compared to non–NPF event days. Morning and late evening/night–time peaks occurred synchronously with peaks in large charged particles. BC is often used as a proxy for traffic–related air pollution and other combustion–related activities (Seinfeld and Pandis, 2016). Peaks in BC were synchronous with peaks in the CS due to the high surface area of BC–containing particles. Maximum H_2SO_4 dimer concentrations peaked synchronously with intermediate charged particle concentrations. In the nitrate CI–APi–ToF, the H_2SO_4 dimer is a representation of atmospheric $H_2SO_4.HSO_4^-$, larger atmospheric sulphuric acid–base clusters which undergo evaporation due to chemical ionisation, and some ion-molecule pairing in the front of the CIMS inlet (Almeida et al., 2013) and is considered a good proxy for the occurrence of NPF in urban environments (Yao et al., 2018). H_2SO_4 dimer is highest on NPF days, while BC is low. BC peaks in the evening-time, possibly due to a shallow nocturnal boundary layer on these days. CS on event days is similar to non-event days, indicating that the key difference is H_2SO_4 dimer source strength. A CS peak approximately five hours after the H_2SO_4 dimer peak on NPF event days reflects the growing mode of new particles contributing appreciably to surface area.

Concentrations of other acids (HIO_3, MSA) are an order of magnitude lower than H_2SO_4 concentrations, and so H_2SO_4 is the most likely candidate for the driver of NPF in this area. Temperatures were high (~30 °C) during the campaign, and it is unlikely that OOMs can drive particle formation in this data (Simon et al., 2020). The correlation between H_2SO_4 dimer and charged particle concentration (**Figure 5**) shows that there is no statistically significant correlation between H_2SO_4 dimer and small charged particles, while the correlation with intermediate and large ions is statistically significant. The correlation is strongest for the intermediate ions, which peak coincidentally with H_2SO_4 dimer, which is coincident with high solar radiation (**Figure 3**, **Figure S3**). Particle formation is accelerated by ionising radiation (Kirkby et al., 2011; Kirkby et al., 2023), and a fraction of these new particles will be charged or will pick up charge as they grow. NPF occurred on days with higher temperatures and solar radiation (**Figure S3**) which is typical for ground-level NPF (Kerminen et al., 2018; Lee et al., 2019). High temperatures can increase cluster evaporation rates, but this can be offset by the presence of ions (Lee et al., 2019) although this is dependent on cluster composition (Kirkby et al., 2023). We attribute these midday peaks in intermediate and large ions to NPF which is likely driven by sulfuric acid, and argue that NPF is the major source of charged particles in this campaign (**Figure 2b**, **Figure S3**). Primary emissions of intermediate and charged ions will be coincident with BC emissions (Thomas et al., 2024)

Undefined and non-NPF days occur when H_2SO_4 dimer is low. Undefined events are seen when CS is high, and BC is higher than NPF event days, likely due to traffic emissions, and non-event days occur when BC and CS are lower. Non-NPF days are possibly observed on these days due to low concentrations of precursors. The morning and evening peaks in intermediate and large ions are coincident with peaks in BC concentrations, and are therefore explicable by primary traffic emissions (Thomas et al., 2024), and we argue that primary emissions are the second largest source of intermediate and large ions in our data.
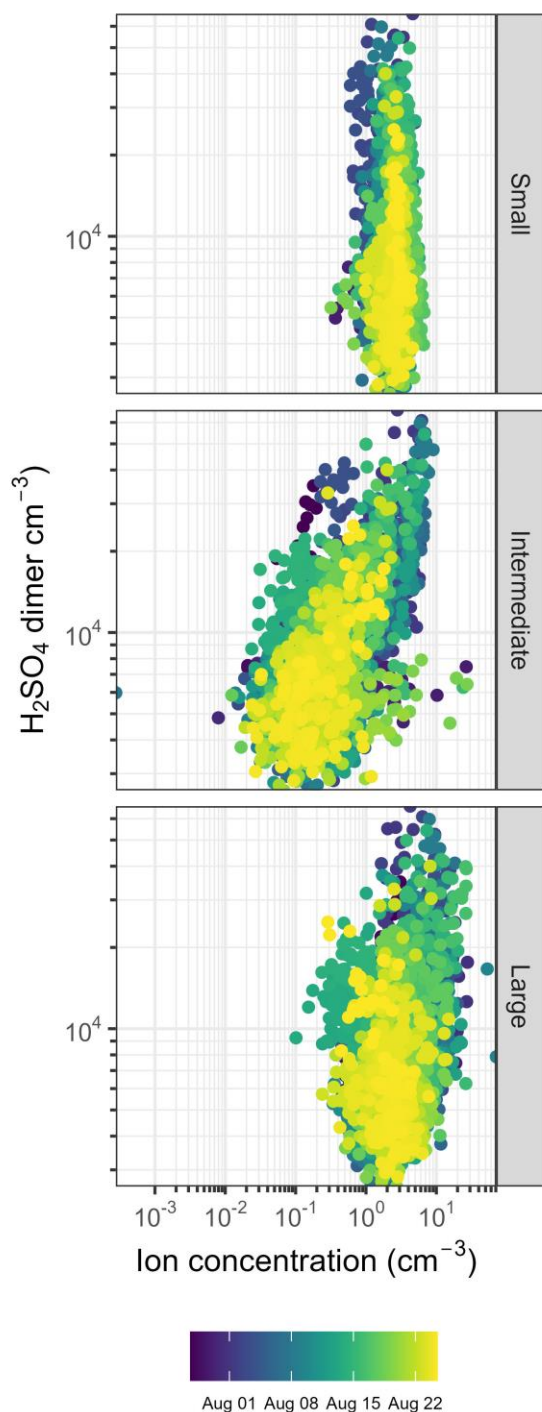
Figure 5: Correlation of H₂SO₄ dimer with small, intermediate, and large ions, coloured by date. The R^2 values are 0.0014, 0.27, and 0.079, respectively, and the p values are >0.05, <0.05, and <0.05, respectively.

3.6. Charged particles and particle formation rates

Figure 6a,b shows the apparent formation rates (J) of 3 and 7.5 nm charged particles (sum of both negative and positive particle formation rates; $J_{3-7.5}^{charged}$ and $J_{7.5-22}^{charged}$) and total particles ($J_{3-7.5}^{total}$ and $J_{7.5-22}^{total}$) during NPF event days at Leipzig–TROPOS. **Figure 6c** shows the

diurnal cycle of these rates. The ratio of $J^{positive}$:$J^{negative}$ is 0.9. Notably, the apparent J values of charged particles increased with aerosol size. The mean J values of 3 and 7.5 nm charged particles during NPF were 0.165 and 0.326 $cm^{-3}\,s^{-1}$, respectively, with mean values of $J_{7.5-22}^{charged}$ approximately 2 times higher than $J_{3-7.5}^{charged}$. These compare with mean J values of 3 and 7.5 nm total particles during NPF of 7.21 and 1.47 $cm^{-3}\,s^{-1}$, respectively, with mean values of $J_{7.5-22}^{total}$ approximately 0.68 times than $J_{3-7.5}^{total}$. The aforementioned J values are within the observed tropospheric ranges for charged and total particles reported by Hirsikko et al. (2011). When considering the calculated ratios of $J^{charged}$ / J^{total} in the respective size ranges, the apparent mean contributions of charged particles to 3 and 7.5 nm total particle formation were 5.7 and 12.7%, respectively. $J_{3-7.5}^{total}$ is higher than $J_{7.5-22}^{total}$, which is typical, as new particles are lost as they grow from 3 to 7.5 nm. However, $J_{3-7.5}^{charged}$ is lower than $J_{7.5-22}^{charged}$. We attribute this to charging of growing aerosol by the condensation of smaller charged particles, and this is consistent with the low concentrations of intermediate charged particles (Figure 2a, Table 1). The diurnal cycle in J shows a peak that is coincident with the peaks in H_2SO_4 dimer (Figure 4) and intermediate charged ion concentrations (Figure 4).

Large charged particles are more likely to act as a sink because of their greater surface area. In comparison, smaller charged particles are more susceptible to ion–ion recombination due to higher mobility. This recombination process, wherein two oppositely charged particles combine and neutralise each other, accounted for in equation (4), can impact the abundance of smaller charged particles, influencing their ability to contribute to nucleation and particle formation in the atmosphere. It would be reasonable to view $J_{3-7.5}^{charged}$ as an upper limit to ion–induced nucleation, while larger charged particles appear to have a substantial contribution from charges acquired subsequently. The apparent contributions are comparable with ranges from other European field sites (1–30%) covering a wide variety of environments reported by Manninen et al. (2010). Nevertheless, observed ratios of charged to total particles in the size range impacted by NPF suggest charged particles play a minor role compared to neutral particles in NPF at Leipzig–TROPOS in our data.
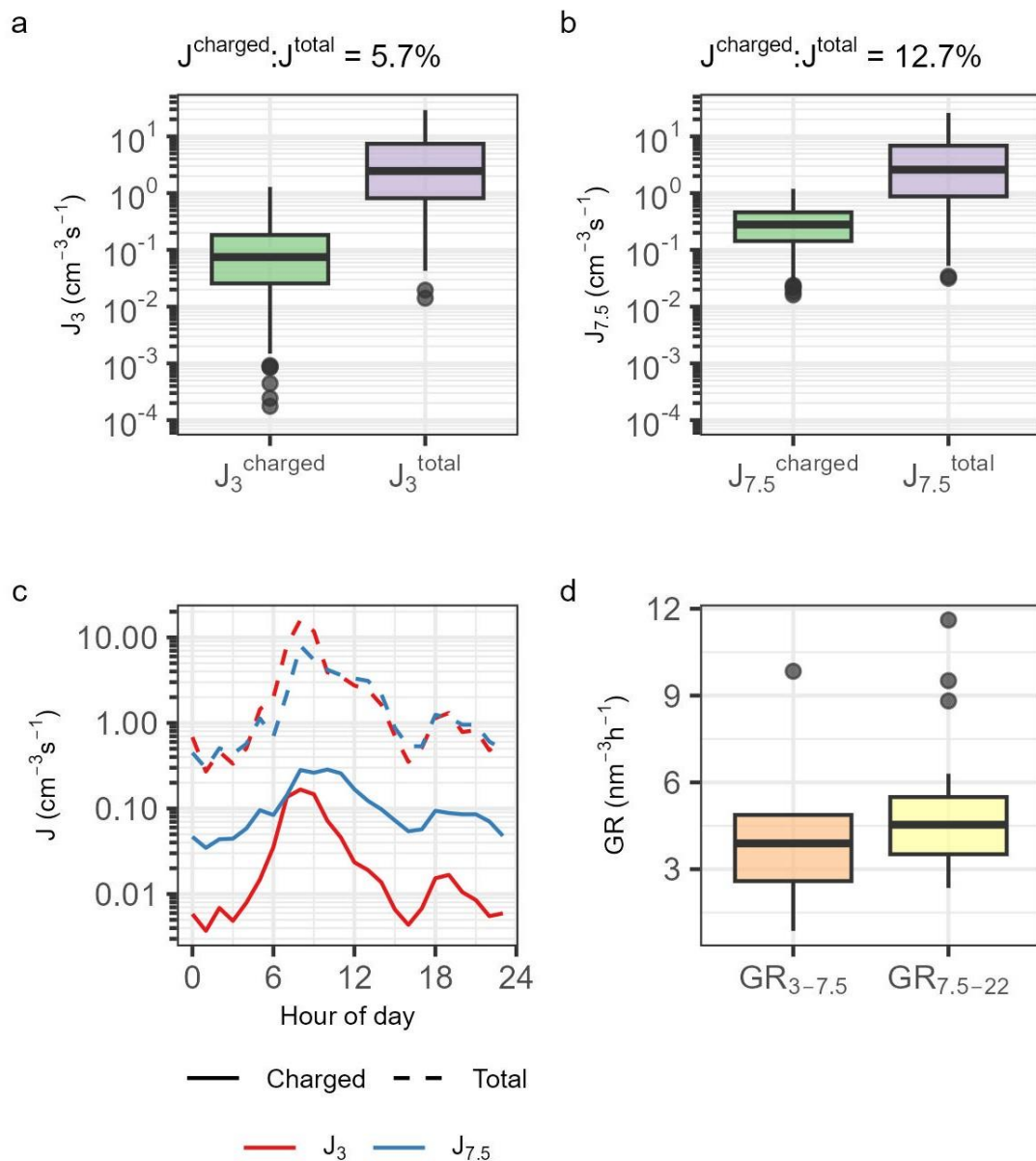
435

Figure 6: Apparent formation rates of (A) 3–7.5 nm charged particles (left) and total particles (right) and (B) 7.5–22 nm charged particles (left) and total particles (right). Calculated from 9 new particle formation (NPF) event days using 10–minute means. (C) the diurnal cycle in formation rates on NPF days, and (D) growth rates (GR) of 3–7.5 and
440 **7.5–22 nm charged particles. The coloured rectangle represents the middle 50% of the data, with the central horizontal line indicating the median value. The whiskers (vertical lines) extending from the rectangle show the spread of the data. Data points beyond the whiskers show outliers.**

3.7. Charged particle growth rates

445 **Figure 6d** shows growth rates (*GR*s) of charged particles within diameters 3–7.5 and 7.5–22

nm during NPF event days at Leipzig–TROPOS. Consistent with previous studies (Manninen

et al., 2010; Dos Santos et al., 2015; Svensmark et al., 2017), the GR of charged particles generally increased with size. This observation is attributed to the Kelvin effect, where the condensational growth of smaller particles is driven by a limited number of very low volatility compounds. In contrast, the growth of larger particles is influenced by a greater number of molecules, including oxygenated organic molecules (Kirkby et al., 2023). Contrary to Js discussed in **section 3.6**, GRs of charged particles are expected to align more closely with that of neutral particles (Svensmark et al., 2017). Small discrepancies may arise due to the enhanced condensation of ionised gases and improved coagulation resulting from charge–charge effects (Svensmark et al., 2017). Mean *GR*s of 3–7.5 and 7.5–22 nm charged particles were 4.0 and 5.2 nm h^{-1}, respectively. In comparison, Manninen et al. (2010) reported median *GR*s from various European field sites as 4.3 and 5.4 nm h^{-1} for 3–7 nm and 7–20 nm charged particles, respectively.

4. CONCLUSION

The charged and total PNSDs were measured from 27th July to 25th August 2022 using NAIS in urban Leipzig to understand the sources, sinks, and dynamics of charged particles. Throughout the measurement campaign, small (0.8–1.6 nm), intermediate (1.6–7.5 nm), and large (7.5–22 nm) charged particles were ever–present. Small charged particle concentrations were consistent with observations in the existing literature. A clear disparity was evident between positive and negative polarities, attributed to the Earth's electrode effect. Despite these differences, their diurnal cycles were very similar. Small charged particle concentrations peaked in the early morning, decreased into the afternoon, and rose again into the night. These fluctuations are believed to be related to changes in the boundary layer mixing height and the accumulation of radioactive gases. Maximum concentrations of intermediate and large charged particles were observed in the morning hours, with the latter peaking closer to midday. Local air pollution had a more substantial impact on larger charged particles compared to small and intermediate charged particles, indicated by synchronous peaks in black carbon concentrations, and we argue that primary emissions are a major contributor to intermediate and large ions.

NPF events were identified on 30% of measurement days, occurring under intense solar radiation, significant diurnal temperature fluctuations, and decreasing relative humidity from morning to afternoon. Notably, small charged particle concentrations were typically lower on NPF event days compared to non–NPF event days. Peak concentrations of intermediate and large

charged particles were approximately 4.0–4.4 and 3.6–3.7 times higher (depending on polarity, higher for negative particles), respectively, on NPF event days compared to non–NPF event days. H_2SO_4 dimer concentrations were elevated on NPF event days and peaked synchronously with intermediate charged particle concentrations.

The apparent contributions of charged particles to 3 and 7.5 nm particle formation were 5.7 and 12.7%, respectively, with mean growth rates of 4.0 and 5.2 nm h^{-1}. Both the apparent formation and growth rates of charged particles increased with aerosol size and were found to be comparable with ranges reported in previous studies. The ratio of total to charged nanoparticles and small magnitude of $J_{3-7.5}^{charged}$ suggest that ion–induced processes play a minor role compared to neutral particles in NPF at Leipzig–TROPOS in this campaign.

DATA AND MATERIALS AVAILABILITY

AUTHOR CONTRIBUTIONS

Conceptualisation – AR, JB; data curation – AR, JB; formal analysis – AR,JB; funding acquisition – RH, ZS; investigation – AR, JB; methodology – AR, JB; project administration – RH; resources – MR, MDM, PM, KW, MM; software – AR, JB; supervision – RH, ZS; visualisation – AR, JB; writing (original draft preparation) – AR; writing (review & editing) – AR, JB, DB, ZS, AK, MR, MDM, PM, KW, RH.

COMPETING INTERESTS

The authors declare that they have no conflict of interest.

ACKNOWLEDGEMENTS

This project was funded by the UK Natural Environment Research Council (grant NE/V001523/1 NPF-Urban). This project has received funding from the European Research Council under the European Union's Horizon 2020 research and innovation programme under Grant No. 101002728 (ERC Consolidator Grant Project ADAPT). Support from the Research Council of Finland (353836 and 346373) and its Flagship program (decision No.'s 337551, 357903) and the Doctoral school of the Faculty of Engineering and Natural Sciences of

Tampere University are gratefully acknowledged. The University of Birmingham would like to express sincere appreciation to TROPOS for their gracious hosting and invaluable assistance during our measurement campaign.

510 **REFERENCES**

Bousiotis, D., Pope, F. D., Beddows, D. C. S., Dall'Osto, M., Massling, A., Nøjgaard, J. K., Nordstrøm, C., Niemi, J. V, Portin, H., Petäjä, T., Perez, N., Alastuey, A., Querol, X., Kouvarakis, G., Mihalopoulos, N., Vratolis, S., Eleftheriadis, K., Wiedensohler, A., Weinhold, K., Merkel, M., Tuch, T. and Harrison, R. M.: A phenomenology of new particle formation

515 (NPF) at 13 European sites, Atmos. Chem. Phys., 21(15), 11905–11925, doi:10.5194/acp-21-11905-2021, 2021.

Boutle, I., Price, J., Kudzotsa, I., Kokkola, H. and Romakkaniemi, S.: Aerosol--fog interaction and the transition to well-mixed radiation fog, Atmos. Chem. Phys., 18(11), 7827–7840, doi:10.5194/acp-18-7827-2018, 2018.

520 Brean, J., Dall'Osto, M., Simó, R., Shi, Z., Beddows, D. C. S. and Harrison, R. M.: Open ocean and coastal new particle formation from sulfuric acid and amines around the Antarctic Peninsula, , doi:10.1038/s41561-021-00751-y, 2021.

Brean, J., Beddows, D. C. S., Harrison, R. M., Song, C., Tunved, P., Ström, J., Krejci, R., Freud, E., Massling, A., Skov, H., Asmi, E., Lupi, A. and Dall'Osto, M.: Collective

525 geographical ecoregions and precursor sources driving Arctic new particle formation, Atmos. Chem. Phys., 23(3), 2183–2198, doi:10.5194/acp-23-2183-2023, 2023.

Cai, R. and Jiang, J.: A new balance formula to estimate new particle formation rate: reevaluating the effect of coagulation scavenging, Atmos. Chem. Phys., 17(20), 12659–12675, doi:10.5194/acp-17-12659-2017, 2017.

530 Carslaw, K. S., Lee, L. A., Reddington, C. L., Pringle, K. J., Rap, A., Forster, P. M., Mann, G. W., Spracklen, D. V, Woodhouse, M. T., Regayre, L. A. and Pierce, J. R.: Large contribution of natural aerosols to uncertainty in indirect forcing, Nature, 503(7474), 67–71, doi:10.1038/nature12674, 2013.

Čeliković, I.; Pantelić, G.; Vukanac, I.; Krneta Nikolić, J.; Živanović, M.; Cinelli, G.; Gruber,

535 V.; Baumann, S.; Quindos Poncela, L.S.; Rabago, D.: Outdoor Radon as a Tool to Estimate Radon Priority Areas—A Literature Overview. Int. J. Environ. Res. Public Health *19*(662), doi:10.3390/ijerph19020662, 2022.

Dal Maso, M., Kulmala, M., Riipinen, I., Wagner, R., Hussein, T., Aalto P., P. and Lehtinen

K., E. J.: Formation and growth of fresh atmospheric aerosols: eight years of aerosol size distribution data from SMEAR II, Hyytiala, Finland, Boreal Environ. Res., 10(5), 323–336, 2005.

Dhanorkar, S. and Kamra, A. K.: Diurnal variation of ionization rate close to ground, J. Geophys. Res. Atmos., 99(D9), 18523–18526, doi:10.1029/94JD01335, 1994.

Gagné, S., Nieminen, T., Kurtén, T., Manninen, H. E., Petäjä, T., Laakso, L., Kerminen, V.-M., Boy, M. and Kulmala, M.: Factors influencing the contribution of ion-induced nucleation in a boreal forest, Finland, Atmos. Chem. Phys., 10(8), 3743–3757, doi:10.5194/acp-10-3743-2010, 2010.

Gagné, S., Leppä, J., Petäjä, T., McGrath, M. J., Vana, M., Kerminen, V.-M., Laakso, L. and Kulmala, M.: Aerosol charging state at an urban site: new analytical approach and implications for ion-induced nucleation, Atmos. Chem. Phys., 12(10), 4647–4666, doi:10.5194/acp-12-4647-2012, 2012.

Gordon, H., Kirkby, J., Baltensperger, U., Bianchi, F., Breitenlechner, M., Curtius, J., Dias, A., Dommen, J., Donahue, N. M., Dunne, E. M., Duplissy, J., Ehrhart, S., Flagan, R. C., Frege, C., Fuchs, C., Hansel, A., Hoyle, C. R., Kulmala, M., Kürten, A., Lehtipalo, K., Makhmutov, V., Molteni, U., Rissanen, M. P., Stozhkov, Y., Tröstl, J., Tsagkogeorgas, G., Wagner, R., Williamson, C., Wimmer, D., Winkler, P. M., Yan, C. and Carslaw, K. S.: Causes and importance of new particle formation in the present-day and preindustrial atmospheres, J. Geophys. Res. Atmos., 122(16), 8739–8760, doi:10.1002/2017JD026844, 2017.

He, X.-C., Tham, Y. J., Dada, L., Wang, M., Finkenzeller, H., Stolzenburg, D., Iyer, S., Simon, M., Kürten, A., Shen, J., Rörup, B., Rissanen, M., Schobesberger, S., Baalbaki, R., Wang, D. S., Koenig, T. K., Jokinen, T., Sarnela, N., Beck, L. J., Almeida, J., Amanatidis, S., Amorim, A., Ataei, F., Baccarini, A., Bertozzi, B., Bianchi, F., Brilke, S., Caudillo, L., Chen, D., Chiu, R., Chu, B., Dias, A., Ding, A., Dommen, J., Duplissy, J., Haddad, I. El, Carracedo, L. G., Granzin, M., Hansel, A., Heinritzi, M., Hofbauer, V., Junninen, H., Kangasluoma, J., Kemppainen, D., Kim, C., Kong, W., Krechmer, J. E., Kvashin, A., Laitinen, T., Lamkaddam, H., Lee, C. P., Lehtipalo, K., Leiminger, M., Li, Z., Makhmutov, V., Manninen, H. E., Marie, G., Marten, R., Mathot, S., Mauldin, R. L., Mentler, B., Möhler, O., Müller, T., Nie, W., Onnela, A., Petäjä, T., Pfeifer, J., Philippov, M., Ranjithkumar, A., Saiz-Lopez, A., Salma, I., Scholz, W., Schuchmann, S., Schulze, B., Steiner, G., Stozhkov, Y., Tauber, C., Tomé, A., Thakur, R. C., Väisänen, O., Vazquez-Pufleau, M., Wagner, A. C., Wang, Y., Weber, S. K., Winkler, P. M., Wu, Y., Xiao, M., Yan, C., Ye, Q., Ylisirniö, A., Zauner-Wieczorek, M., Zha, Q., Zhou, P., Flagan, R. C., Curtius, J., Baltensperger, U., Kulmala, M., Kerminen, V.-M.,

Kurtén, T., et al.: Role of iodine oxoacids in atmospheric aerosol nucleation, Science (80-.)., 371(6529), 589–595, doi:10.1126/science.abe0298, 2021.

575   Hirsikko, A., Nieminen, T., Gagné, S., Lehtipalo, K., Manninen, H. E., Ehn, M., Hõrrak, U., Kerminen, V.-M., Laakso, L., McMurry, P. H., Mirme, A., Mirme, S., Petäjä, T., Tammet, H., Vakkari, V., Vana, M. and Kulmala, M.: Atmospheric ions and nucleation: a review of observations, Atmos. Chem. Phys., 11(2), 767–798, doi:10.5194/acp-11-767-2011, 2011.

Hoppel, W. A.: Theory of the electrode effect, J. Atmos. Terr. Phys., 29(6), 709–721, 580   doi:https://doi.org/10.1016/0021-9169(67)90215-2, 1967.

Hõrrak, U.: Statistical results of air ions and aerosol measurements on the island of Vilsandi in the summer of 1984, Acta Comm. Univ. Tartu, 755, 47–57, 1987.

Hõrrak, U., Salm, J. and Tammet, H.: Diurnal variation in the concentration of air ions of different mobility classes in a rural area, J. Geophys. Res. Atmos., 108(D20), 585   doi:10.1029/2002JD003240, 2003.

J-P Borra, R A Roos, D Renard, H Lazar, A Goldman and M Goldman: Electrical and chemical consequences of point discharges in a forest during a mist and a thunderstorm, J. Phys. D. Appl. Phys., 30(1), 84, doi:10.1088/0022-3727/30/1/011, 1997.

Jayaratne, E. R., Ling, X. and Morawska, L.: Ions in motor vehicle exhaust and their dispersion 590   near busy roads, Atmos. Environ., 44(30), 3644–3650, doi:10.1016/j.atmosenv.2010.06.043, 2010.

Jayaratne, E. R., Ling, X. and Morawska, L.: Corona ions from high-voltage power lines: Nature of emission and dispersion, J. Electrostat., 69(3), 228–235, doi:10.1016/j.elstat.2011.03.014, 2011.

595   Jayaratne, E. R., Ling, X. and Morawska, L.: Observation of ions and particles near busy roads using a neutral cluster and air ion spectrometer (NAIS), Atmos. Environ., 84, 198–203, doi:10.1016/j.atmosenv.2013.11.045, 2014.

Jiang, S.-Y., Ma, A. and Ramachandran, S.: Negative Air Ions and Their Effects on Human Health and Air Quality Improvement., Int. J. Mol. Sci., 19(10), doi:10.3390/ijms19102966, 600   2018.

Kelly, F. J. and Fussell, J. C.: Air pollution and public health: emerging hazards and improved understanding of risk, Environ. Geochem. Health, 37(4), 631–649, doi:10.1007/s10653-015-9720-1, 2015.

Kerminen, V. M., Chen, X., Vakkari, V., Petäjä, T., Kulmala, M. and Bianchi, F.: Atmospheric 605   new particle formation and growth: Review of field observations, Environ. Res. Lett., 13(10), doi:10.1088/1748-9326/aadf3c, 2018.

Kirkby, J., Curtius, J., Almeida, J., Dunne, E., Duplissy, J., Ehrhart, S., Franchin, A., Gagné, S., Ickes, L., Kürten, A., Kupc, A., Metzger, A., Riccobono, F., Rondo, L., Schobesberger, S., Tsagkogeorgas, G., Wimmer, D., Amorim, A., Bianchi, F., Breitenlechner, M., David, A.,

610   Dommen, J., Downard, A., Ehn, M., Flagan, R. C., Haider, S., Hansel, A., Hauser, D., Jud, W., Junninen, H., Kreissl, F., Kvashin, A., Laaksonen, A., Lehtipalo, K., Lima, J., Lovejoy, E. R., Makhmutov, V., Mathot, S., Mikkilä, J., Minginette, P., Mogo, S., Nieminen, T., Onnela, A., Pereira, P., Petäjä, T., Schnitzhofer, R., Seinfeld, J. H., Sipilä, M., Stozhkov, Y., Stratmann, F., Tomé, A., Vanhanen, J., Viisanen, Y., Vrtala, A., Wagner, P. E., Walther, H., Weingartner, E.,

615   Wex, H., Winkler, P. M., Carslaw, K. S., Worsnop, D. R., Baltensperger, U. and Kulmala, M.: Role of sulphuric acid, ammonia and galactic cosmic rays in atmospheric aerosol nucleation, Nature, 476(7361), 429–433, doi:10.1038/nature10343, 2011.

Kirkby, J., Amorim, A., Baltensperger, U., Carslaw, K. S., Christoudias, T., Curtius, J., Donahue, N. M., Haddad, I. E., Flagan, R. C., Gordon, H., Hansel, A., Harder, H., Junninen,

620   H., Kulmala, M., Kürten, A., Laaksonen, A., Lehtipalo, K., Lelieveld, J., Möhler, O., Riipinen, I., Stratmann, F., Tomé, A., Virtanen, A., Volkamer, R., Winkler, P. M., and Worsnop, D. R.: Atmospheric new particle formation from the CERN CLOUD experiment, Nature Geoscience, 16, 948-957, 10.1038/s41561-023-01305-0, 2023.

Kulmala, M., Riipinen, I., Nieminen, T., Hulkkonen, M., Sogacheva, L., Manninen, H. E.,

625   Paasonen, P., Petäjä, T., Dal Maso, M., Aalto, P. P., Viljanen, A., Usoskin, I., Vainio, R., Mirme, S., Mirme, A., Minikin, A., Petzold, A., Hõrrak, U., Plaß-Dülmer, C., Birmili, W., and Kerminen, V.-M.: Atmospheric data over a solar cycle: no connection between galactic cosmic rays and new particle formation, Atmos. Chem. Phys., 10, 1885–1898, https://doi.org/10.5194/acp-10-1885-2010, 2010.

630   Ku, B. K., & de la Mora, J. F. Relation between Electrical Mobility, Mass, and Size for Nanodrops 1–6.5 nm in Diameter in Air. *Aerosol Science and Technology*, *43*(3), 241–249. doi:10.1080/02786820802590510, 2009.

Kulmala, M., Petäjä, T., Nieminen, T., Sipilä, M., Manninen, H. E., Lehtipalo, K., Dal Maso, M., Aalto, P. P., Junninen, H., Paasonen, P., Riipinen, I., Lehtinen, K. E. J., Laaksonen, A. and

635   Kerminen, V.-M.: Measurement of the nucleation of atmospheric aerosol particles, Nat. Protoc., 7(9), 1651–1667, doi:10.1038/nprot.2012.091, 2012.

Kürten, A., Rondo, L., Ehrhart, S. and Curtius, J.: Calibration of a Chemical Ionization Mass Spectrometer for the Measurement of Gaseous Sulfuric Acid, J. Phys. Chem. A, 116(24), 6375–6386, doi:10.1021/jp212123n, 2012.

640   Lee, S. H., Gordon, H., Yu, H., Lehtipalo, K., Haley, R., Li, Y. and Zhang, R.: New Particle

Formation in the Atmosphere: From Molecular Clusters to Global Climate, J. Geophys. Res. Atmos., doi:10.1029/2018JD029356, 2019.

Mahfouz, N. G. A. and Donahue, N. M.: Technical note: The enhancement limit of coagulation scavenging of small charged particles, Atmos. Chem. Phys., 21(5), 3827–3832, doi:10.5194/acp-21-3827-2021, 2021.

Manninen, H. E., Nieminen, T., Asmi, E., Gagné, S., Häkkinen, S., Lehtipalo, K., Aalto, P., Vana, M., Mirme, A., Mirme, S., Hõrrak, U., Plass-Dülmer, C., Stange, G., Kiss, G., Hoffer, A., Törő, N., Moerman, M., Henzing, B., de Leeuw, G., Brinkenberg, M., Kouvarakis, G. N., Bougiatioti, A., Mihalopoulos, N., O'Dowd, C., Ceburnis, D., Arneth, A., Svenningsson, B., Swietlicki, E., Tarozzi, L., Decesari, S., Facchini, M. C., Birmili, W., Sonntag, A., Wiedensohler, A., Boulon, J., Sellegri, K., Laj, P., Gysel, M., Bukowiecki, N., Weingartner, E., Wehrle, G., Laaksonen, A., Hamed, A., Joutsensaari, J., Petäjä, T., Kerminen, V.-M. and Kulmala, M.: EUCAARI ion spectrometer measurements at 12 European sites – analysis of new particle formation events, Atmos. Chem. Phys., 10(16), 7907–7927, doi:10.5194/acp-10-7907-2010, 2010.

Mercer, J., Wilson, B. Daily Variation of Cosmic Rays. Nature 208, 477–479 (1965). https://doi.org/10.1038/208477a0

Mikhailov, A.: Turbo, An Improved Rainbow Colormap for Visualization, Google Res. Blog [online] Available from: https://blog.research.google/2019/08/turbo-improved-rainbow-colormap-for.html, 2019.

Mirme, S. and Mirme, A.: The mathematical principles and design of the NAIS – a spectrometer for the measurement of cluster ion and nanometer aerosol size distributions, Atmos. Meas. Tech., 6(4), 1061–1071, doi:10.5194/amt-6-1061-2013, 2013.

Pushpawela, B., Jayaratne, R. and Morawska, L.: Temporal distribution and other characteristics of new particle formation events in an urban environment, Environ. Pollut., 233, 552–560, doi:10.1016/j.envpol.2017.10.102, 2018.

Quaas, J., Ming, Y., Menon, S., Takemura, T., Wang, M., Penner, J. E., Gettelman, A., Lohmann, U., Bellouin, N., Boucher, O., Sayer, A. M., Thomas, G. E., McComiskey, A., Feingold, G., Hoose, C., Kristjánsson, J. E., Liu, X., Balkanski, Y., Donner, L. J., Ginoux, P. A., Stier, P., Grandey, B., Feichter, J., Sednev, I., Bauer, S. E., Koch, D., Grainger, R. G., Kirkevåg, A., Iversen, T., Seland, Ø., Easter, R., Ghan, S. J., Rasch, P. J., Morrison, H., Lamarque, J.-F., Iacono, M. J., Kinne, S. and Schulz, M.: Aerosol indirect effects – general circulation model intercomparison and evaluation with satellite data, Atmos. Chem. Phys., 9(22), 8697–8717, doi:10.5194/acp-9-8697-2009, 2009.

675   Rose, C., Foucart, B., Picard, D., Colomb, A., Metzger, J.-M., Tulet, P. and Sellegri, K.: New particle formation in the volcanic eruption plume of the Piton de la Fournaise: specific features from a long-term dataset, Atmos. Chem. Phys., 19(20), 13243–13265, doi:10.5194/acp-19-13243-2019, 2019.

      Dos Santos, V. N., Herrmann, E., Manninen, H. E., Hussein, T., Hakala, J., Nieminen, T.,
680   Aalto, P. P., Merkel, M., Wiedensohler, A., Kulmala, M., Petäjä, T. and Hämeri, K.: Variability of air ion concentrations in urban Paris, Atmos. Chem. Phys., 15(23), 13717–13737, doi:10.5194/acp-15-13717-2015, 2015.

      Seinfeld, J.H. and Pandis, S.N. (2016) Atmospheric Chemistry and Physics: From Air Pollution to Climate Change. John Wiley & Sons, Hoboken.

685   Simon, M., Dada, L., Heinritzi, M., Scholz, W., Stolzenburg, D., Fischer, L., Wagner, A. C., Kürten, A., Rörup, B., He, X.-C., Almeida, J., Baalbaki, R., Baccarini, A., Bauer, P. S., Beck, L., Bergen, A., Bianchi, F., Bräkling, S., Brilke, S., Caudillo, L., Chen, D., Chu, B., Dias, A., Draper, D. C., Duplissy, J., El-Haddad, I., Finkenzeller, H., Frege, C., Gonzalez-Carracedo, L., Gordon, H., Granzin, M., Hakala, J., Hofbauer, V., Hoyle, C. R., Kim, C., Kong, W.,
690   Lamkaddam, H., Lee, C. P., Lehtipalo, K., Leiminger, M., Mai, H., Manninen, H. E., Marie, G., Marten, R., Mentler, B., Molteni, U., Nichman, L., Nie, W., Ojdanic, A., Onnela, A., Partoll, E., Petäjä, T., Pfeifer, J., Philippov, M., Quéléver, L. L. J., Ranjithkumar, A., Rissanen, M. P., Schallhart, S., Schobesberger, S., Schuchmann, S., Shen, J., Sipilä, M., Steiner, G., Stozhkov, Y., Tauber, C., Tham, Y. J., Tomé, A. R., Vazquez-Pufleau, M., Vogel, A. L.,
695   Wagner, R., Wang, M., Wang, D. S., Wang, Y., Weber, S. K., Wu, Y., Xiao, M., Yan, C., Ye, P., Ye, Q., Zauner-Wieczorek, M., Zhou, X., Baltensperger, U., Dommen, J., Flagan, R. C., Hansel, A., Kulmala, M., Volkamer, R., Winkler, P. M., Worsnop, D. R., Donahue, N. M., Kirkby, J., and Curtius, J.: Molecular understanding of new-particle formation from α-pinene between -50 and $+25\,°C$, Atmos. Chem. Phys., 20, 9183–9207, https://doi.org/10.5194/acp-
700   20-9183-2020, 2020.

      Spracklen, D. V, Carslaw, K. S., Merikanto, J., Mann, G. W., Reddington, C. L., Pickering, S., Ogren, J. A., Andrews, E., Baltensperger, U., Weingartner, E., Boy, M., Kulmala, M., Laakso, L., Lihavainen, H., Kivekäs, N., Komppula, M., Mihalopoulos, N., Kouvarakis, G., Jennings, S. G., O'Dowd, C., Birmili, W., Wiedensohler, A., Weller, R., Gras, J., Laj, P., Sellegri, K.,
705   Bonn, B., Krejci, R., Laaksonen, A., Hamed, A., Minikin, A., Harrison, R. M., Talbot, R. and Sun, J.: Explaining global surface aerosol number concentrations in terms of primary emissions and particle formation, Atmos. Chem. Phys., 10(10), 4775–4793, doi:10.5194/acp-10-4775-2010, 2010.

Suni, T., Kulmala, M., Hirsikko, A., Bergman, T., Laakso, L., Aalto, P. P., Leuning, R., Cleugh,

710   H., Zegelin, S., Hughes, D., van Gorsel, E., Kitchen, M., Vana, M., Hõrrak, U., Mirme, S., Mirme, A., Sevanto, S., Twining, J. and Tadros, C.: Formation and characteristics of ions and charged aerosol particles in a native Australian Eucalypt forest, Atmos. Chem. Phys., 8(1), 129–139, doi:10.5194/acp-8-129-2008, 2008.

Svensmark, H., Enghoff, M. B., Shaviv, N. J. and Svensmark, J.: Increased ionization supports

715   growth of aerosols into cloud condensation nuclei, Nat. Commun., 8(1), 2199, doi:10.1038/s41467-017-02082-2, 2017.

Tammet, H.: Continuous scanning of the mobility and size distribution of charged clusters and nanometer particles in atmospheric air and the Balanced Scanning Mobility Analyzer BSMA, Atmos. Res., 82(3), 523–535, doi:10.1016/j.atmosres.2006.02.009, 2006.

720   Tammet, H., Hõrrak, U., Laakso, L. and Kulmala, M.: Factors of air ion balance in a coniferous forest according to measurements in Hyytiälä, Finland, Atmos. Chem. Phys., 6(11), 3377–3390, doi:10.5194/acp-6-3377-2006, 2006.

Tammet, H., Hõrrak, U. and Kulmala, M.: Negatively charged nanoparticles produced by splashing of water, Atmos. Chem. Phys., 9(2), 357–367, doi:10.5194/acp-9-357-2009, 2009.

725   Tammet, H., Komsaare, K. and Hõrrak, U.: Intermediate ions in the atmosphere, Atmos. Res., 135–136, 263–273, doi:10.1016/j.atmosres.2012.09.009, 2014.

Thomas, A. E., Bauer, P. S., Dam, M., Perraud, V., Wingen, L. M., and Smith, J. N.: Automotive braking is a source of highly charged aerosol particles, Proceedings of the National Academy of Sciences, 121, e2313897121, doi:10.1073/pnas.2313897121, 2024.

730   Tian, M., Wang, H., Chen, Y., Yang, F., Zhang, X., Zou, Q., Zhang, R., Ma, Y. and He, K.: Characteristics of aerosol pollution during heavy haze events in Suzhou, China, Atmos. Chem. Phys., 16(11), 7357–7371, doi:10.5194/acp-16-7357-2016, 2016.

Uusitalo, H., Kontkanen, J., Ylivinkka, I., Ezhova, E., Demakova, A., Arshinov, M. Y., Belan, B. D., Davydov, D., Ma, N., Petäjä, T., Wiedensohler, A., Kulmala, M. and Nieminen, T.:

735   Occurrence of new particle formation events in Siberian and Finnish boreal forest, Atmos. Chem. Phys., 1–21, 2021.

Vana, M., Ehn, M., Petäjä, T., Vuollekoski, H., Aalto, P., de Leeuw, G., Ceburnis, D., O'Dowd, C. D. and Kulmala, M.: Characteristic features of air ions at Mace Head on the west coast of Ireland, Atmos. Res., 90(2), 278–286, doi:https://doi.org/10.1016/j.atmosres.2008.04.007,

740   2008.

Wang, J. and Li, S.: Changes in negative air ions concentration under different light intensities and development of a model to relate light intensity to directional change, J. Environ. Manage.,

90(8), 2746–2754, doi:https://doi.org/10.1016/j.jenvman.2009.03.003, 2009.

Wang, Y., Zhuang, G., Tang, A., Yuan, H., Sun, Y., Chen, S. and Zheng, A.: The ion chemistry
745   and the source of PM2.5 aerosol in Beijing, Atmos. Environ., 39(21), 3771–3784, doi:https://doi.org/10.1016/j.atmosenv.2005.03.013, 2005.

Wiedensohler, A., Birmili, W., Nowak, A., Sonntag, A., Weinhold, K., Merkel, M., Wehner, B., Tuch, T., Pfeifer, S., Fiebig, M., Fjäraa, A. M., Asmi, E., Sellegri, K., Depuy, R., Venzac, H., Villani, P., Laj, P., Aalto, P., Ogren, J. A., Swietlicki, E., Williams, P., Roldin, P., Quincey,
750   P., Hüglin, C., Fierz-Schmidhauser, R., Gysel, M., Weingartner, E., Riccobono, F., Santos, S., Grüning, C., Faloon, K., Beddows, D., Harrison, R., Monahan, C., Jennings, S. G., O'Dowd, C. D., Marinoni, A., Horn, H. G., Keck, L., Jiang, J., Scheckman, J., McMurry, P. H., Deng, Z., Zhao, C. S., Moerman, M., Henzing, B., De Leeuw, G., Löschau, G. and Bastian, S.: Mobility particle size spectrometers: Harmonization of technical standards and data structure
755   to facilitate high quality long-term observations of atmospheric particle number size distributions, Atmos. Meas. Tech., 5(3), 657–685, doi:10.5194/amt-5-657-2012, 2012.

Yao, L., Garmash, O., Bianchi, F., Zheng, J., Yan, C., Kontkanen, J., Junninen, H., Mazon, S. B., Ehn, M., Paasonen, P., Sipilä, M., Wang, M., Wang, X., Xiao, S., Chen, H., Lu, Y., Zhang, B., Wang, D., Fu, Q., Geng, F., Li, L., Wang, H., Qiao, L., Yang, X., Chen, J., Kerminen, V.
760   M., Petäjä, T., Worsnop, D. R., Kulmala, M. and Wang, L.: Atmospheric new particle formation from sulfuric acid and amines in a Chinese megacity, Science (80-.)., 361(6399), 278–281, doi:10.1126/science.aao4839, 2018.

Zauner-Wieczorek, M., Curtius, J. and Kürten, A.: The ion–ion recombination coefficient α: comparison of temperature- and pressure-dependent parameterisations for the troposphere and
765   stratosphere, Atmos. Chem. Phys., 22(18), 12443–12465, doi:10.5194/acp-22-12443-2022, 2022.

Zhang, K., Feichter, J., Kazil, J., Wan, H., Zhuo, W., Griffiths, A. D., Sartorius, H., Zahorowski, W., Ramonet, M., Schmidt, M., Yver, C., Neubert, R. E. M. and Brunke, E.-G.: Radon activity in the lower troposphere and its impact on ionization rate: a global estimate
770   using different radon emissions, Atmos. Chem. Phys., 11(15), 7817–7838, doi:10.5194/acp-11-7817-2011, 2011.